High-Efficiency Frequency Conversion through Pulsed-Source Bragg Scattering Four-Wave Mixing in a Silicon Waveguide

Michael Murdock

A senior thesis submitted to the faculty of
Brigham Young University
in partial fulfillment of the requirements for the degree of

Bachelor of Science

Nils Otterstrom, John Colton, Advisors

Department of Physics and Astronomy

Brigham Young University

ABSTRACT

High-Efficiency Frequency Conversion through Pulsed-Source
Bragg Scattering Four-Wave Mixing in a Silicon Waveguide

Michael Murdock
Department of Physics and Astronomy, BYU
Bachelor of Science

Here we demonstrate high-efficiency frequency conversion in a silicon waveguide through Bragg Scattering Four-Wave Mixing (BSFWM). Conversion efficiency of 18% is reached without accounting for nonlinear loss. The signal and both pump lasers are synchronously pulsed with a repetition period longer than and pulse duration much shorter than the free carrier lifetime. This reduces nonlinear loss from free carrier absorption while still reaching peak pump powers of 300 mW on-chip. We discuss the advantages and limitations of this approach and how it could be refined to reach unity-level conversion efficiency.

Keywords: Four-Wave Mixing, Silicon Photonics, Nonlinear Optics, Bragg Scattering Four-Wave Mixing, Four-Wave Mixing Bragg Scattering, BSFWM, FWM-BS

ACKNOWLEDGMENTS

I would like to express my gratitude to my research advisor, Nils Otterstrom. He has patiently helped me—from a fledgling beginning—to understand nonlinear optics and learn the habits of high-quality scientific research and writing. He has born my countless questions (and repeated questions) with patience and enthusiasm. He has freely given of his time far more than his job duties would have required, counseling with me in career decisions, pointing me to job opportunities, and helping me to realize a clearer vision of myself and my future. This work builds upon his work in [1] and [2] and was only possible because of his vision, technical understanding, and creativity.

I especially want to express gratitude to my wife. She has encouraged and lifted me through this entire writing process and helped me get through many a rough, downcast moment. Many times, I have owed my motivation to keep pushing forward to her encouragement and love.

This material is based upon work supported by the Laboratory Directed Research and Development program at Sandia National Laboratories. Sandia National Laboratories is a multi-program laboratory managed and operated by National Technology and Engineering Solutions of Sandia, LLC., a wholly owned subsidiary of Honeywell International, Inc., for the U.S. Department of Energy's National Nuclear Security Administration under Contract No. DE-NA-0003525 (SAND2024-...). This work describes objective technical results and analysis. Any subjective views or opinions that might be expressed herein do not necessarily represent the views of the U.S. Department of Energy or the United States Government.

Contents

List of Figures

Chapter 1

Introduction and Background

In silicon photonics, nonlinear loss is one of the primary impediments to achieving high-efficiency all-optical frequency conversion. At telecom wavelengths, nonlinear loss is caused by two phenomena. First, two-photon absorption (TPA), where the absorption of two photons excites an electron from the valence band to the conduction band, becoming a free carrier. Second, TPA-induced free carrier absorption (FCA), where the conduction-band electron absorbs single photons. Both sources of loss become increasingly detrimental as optical power increases. In this work, we demonstrate the mitigation of TPA-induced FCA loss by creating a picosecond pulsed laser source that exploits the short lifetime of free carriers. We show experimentally that such a scheme results in record high frequency conversion efficiency in silicon photonic waveguides. This is demonstrated using the nonlinear optical process known as Bragg Scattering Four-Wave Mixing (BSFWM) in a silicon-on-insulator waveguide.

1.1 Motivation

Optical processes such as frequency conversion have applications in both classical and quantum systems. When these processes can be made all-optical, they offer the promise of overcoming

electronic bottleneck, reducing noise, and increasing communication rates [3]. As an example in quantum systems, frequency conversion is an important tool needed at interfaces requiring differing photon wavelengths such as those connecting photonic quantum systems with acoustic or atomic ones. In classical systems, all-optical frequency conversion, which could be realized within a single integrated photonic chip, offers a smaller footprint, low cost, and lower power consumption than non-integrated solutions [3].

An important step towards realizing useful all-optical applications is the achievement of higher frequency conversion efficiencies. BSFWM is one of several four-wave mixing (FWM) processes that can be used for all-optical frequency conversion. However, as will be discussed in Section 1.2, BSFWM has the unique advantage of being inherently low noise and thereby preserving quantum states [4, 5].

Realizing high efficiencies can be difficult. One of the primary impediments is nonlinear loss, which becomes detrimental as pump powers are increased to the levels necessary for high-efficiency conversion. As discussed in Otterstrom 2021 [2], nonlinear loss can be mitigated through a pulsed laser technique. To understand this, we must understand the physical background of BSFWM and nonlinear loss.

1.2 Physical Background: Bragg Scattering Four-Wave Mixing and Nonlinear Loss

1.2.1 Nonlinear Optics and Bragg Scattering Four-Wave Mixing

At high enough optical powers—such as those produced by laser light—the incident laser light may significantly modify the optical properties of the material through which it propagates. This is the realm of nonlinear optics. The response of the material to the light has components that scale linearly

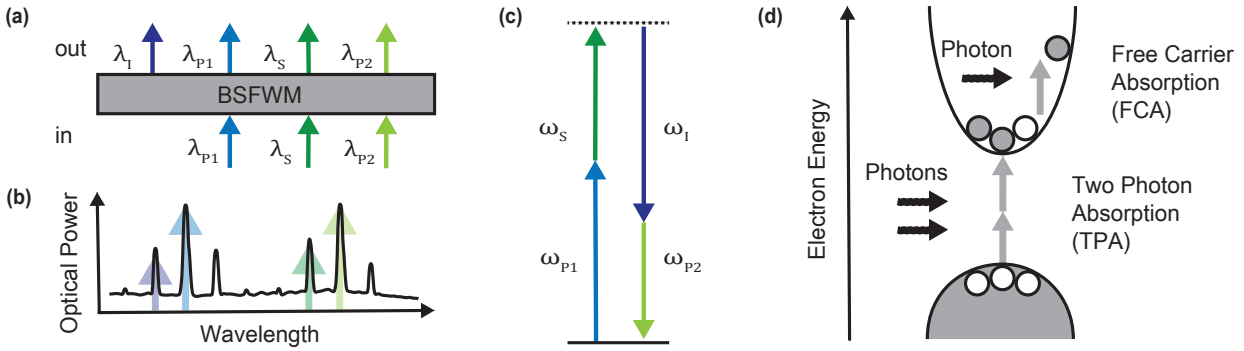

Figure 1.1 Bragg Scattering Four-Wave Mixing (BSFWM) and Nonlinear Loss. ***(a)*** *BSFWM as a simplistic "black box" into which light at three wavelengths enters a photonic material: two strong pump wavelengths and a signal wavelength. They mix in the material and the result is conversion of some of the light to a fourth wavelength: the idler.* ***(b)*** *Example wavelength spectra for BSFWM.* ***(c)*** *Energy conservation for BSFWM.* ***(d)*** *Electron energy diagram of two-photon absorption (TPA) and free carrier absorption (FCA).*

(first order), quadratically (second order), and at higher orders with the strength of the optical field from the applied light; it is in this way that a material's response—and the associated nonlinear optical phenomena—are "nonlinear." Second order responses occur only certain materials, but third-order responses can occur in all optical mediums [6]. Some materials—such as silicon—have a much larger third-order response than do other materials. This research was done in silicon and focused exclusively on Bragg Scattering Four-Wave Mixing, which is a third order nonlinear optical process, meaning it occurs as a result of third-order nonlinear optical responses in the silicon.

In BSFWM in this experiment, the light incident on the silicon waveguide contains three frequencies: two high-power "pump" frequencies and a "signal" frequency. As shown in Fig. 1.1 (a-c), in BSFWM light at the signal wavelength mixes with high-power light at the first pump wavelength and is converted to light at a new "idler" wavelength and the second pump wavelength. The efficiency with which signal light is converted to idler light is proportional to the product of the powers of the two pumps. Thus, at low pump powers, conversion becomes negligible and almost no idler light is produced. At high pump powers, conversion occurs and idler light is produced. If

pump power is high enough, signal power can become noticeably depleted because a significant fraction of signal light is converted to the idler frequency.

Figure 1.1 (c) shows the energy conservation of BSFWM. Photon by photon, light is converted from one side-band (the signal wavelength) to another (the idler wavelength). Because the total side-band power stays constant, vacuum fluctuations associated with the side-bands are not amplified and BSFWM is an inherently noiseless process [5]. This gives it the unique low-noise and quantum state preserving advantages mentioned in Section 1.1.

Other FWM interactions involving two pumps can be seen in the plots in Fig. 1.1 (b) in the form of the additional peaks in the black plot which do not correspond to the pumps (blue and light green), signal (dark green) or idler (purple). In these other FWM interactions–such as the modulation interaction (two photons from a single pump combining to produce side-bands on either side of itself) and phase-conjugation process (one photon from each pump combining to produce a signal and an idler photon)–pump photons are destroyed in pairs and side-band (signal and idler) photons are produced in pairs. This behavior enables vacuum fluctuations to be amplified and excess noise is produced. The lack of this excess noise in BSFWM suggests its usefulness especially for frequency conversion in few-photon (quantum) systems. For more information, see McKinstrie 2005 [5].

1.2.2 Nonlinear Loss

Increasing the conversion efficiency through optical mixing processes such as BSFWM necessarily requires elevated optical power. As optical power increases, nonlinear loss effects also become more prevalent and more detrimental. To understand the effect of nonlinear loss, consider the differential equation that captures propagation loss in silicon waveguides:

$$\frac{dP}{dz} = -\alpha P - \beta P^2 - \gamma P^3 \tag{1.1}$$

In this equation, α is the linear loss coefficient and β and γ are nonlinear loss coefficients. Linear loss is caused by the physical design of the waveguide and the choice of material, whereas nonlinear loss is caused by (1) two-photon absorption (TPA), which is captured in the coefficient β and (2) TPA-induced free carrier absorption (FCA), whose magnitude is represented by the coefficient γ. This equation is taken from the supplementary information of Kittlaus 2016 [7]. Here, P represents the optical power as a function of distance z traversed within the waveguide. Because TPA-induced FCA scales as the cube of the optical power, this source of loss rapidly becomes detrimental as we attempt to increase the optical power and the corresponding conversion efficiency.

TPA-induced FCA is illustrated in Fig. 1.1 (d). Two telecom-frequency photons have enough combined energy to promote an electron in silicon from the valence band into the conduction band (two-photon absorption), where the hole it leaves behind and the electron itself become free carriers. The free carriers can repeatedly absorb single photons (free carrier absorption), dramatically attenuating pump power when the input power is high enough. This large reduction of pump powers correspondingly reduces the amount of frequency conversion that occurs.

1.3 Methodology and Results

Loss from TPA-induced FCA can be reduced by taking advantage of the short lifetime of free carriers (about 1 ns). If optical pulses are produced at a pulse repetition period longer than the free carrier lifetime (5-10 ns, for example) and with a pulse duration much shorter than that lifetime (100-200 ps), free carriers fall back into the valence band before the subsequent pulse arrives. This dramatically reduces the probability that incoming photons will collide with and be absorbed by free carriers, and thus curtails this source of loss. This technique has been demonstrated previously, showing reduced TPA-induced FCA loss with little device degradation despite the high peak powers [2, 8, 9].

Many commercially available laser sources can produce the needed combinations of pulse width and repetition rate. Others offer widely varying wavelengths, and some can both vary the wavelength and the pulse timing parameters. But few, if any, commercial laser systems can produce multiple synchronized pulses at different wavelengths, while permitting simultaneous tuning of parameters such as pulse width, repetition rate, wavelength, optical intensity, and time-synchronization or de-synchronization. And yet, access to full customization of all these parameters enables more complete characterization of nonlinear optical processes.

Here, we build a custom laser source capable of satisfying this wide range of requirements. We show that such a source can produce synchronized pulses with durations as short as hundreds of picoseconds for at least three wavelengths simultaneously. The pulses can be de-synchronized from each other by up to 560 ps, and wavelengths for each can be chosen anywhere within the telecom C-band. Pulse width and repetition rate can be tuned at will, ranging from hundreds of picoseconds to tens of nanoseconds, with extinction ratios above 20 dB and on-chip peak powers above 300 mW readily achievable. We demonstrate that by using such a source, coupled to a low-loss silicon-on-insulator waveguide, on-chip conversion efficiencies of at least 18% can be achieved. We then discuss how this pulsed source could be improved to reach watt-level peak powers on-chip, where frequency conversion could reach near-unity values.

Chapter 2

Methods and Results

In Section 2.1 of this chapter, the tunable pulsed laser source built for and used in this experiment is outlined, capable of meeting the broad requirements (see Section 1.3) necessary for full BSFWM characterization. In Section 2.2 a specially-designed low-loss waveguide is described, capable of high optical efficiencies at telecom wavelengths. In Section 2.3, details are given of the semi-automated data collection and analysis processes used to characterize BSFWM in this waveguide across a spectrum of pump powers and pulse delays. Finally, in Section 2.4, conversion efficiency results are given, demonstrating a good fit to theoretical predictions.

2.1 A Tunable Pulsed Laser Source

A schematic of the experimental layout is shown in Fig. 2.1. The custom pulsed source comprises all elements prior to the silicon waveguide. Two telecom c-band laser sources (the pumps) emit light at 1550 nm and 1560 nm. These pass through independent polarization controllers (PC) and couple together in a 50-50 fiber splitter. They are then amplified to 20 dBm through an erbium doped fiber amplifier (EDFA) and enter a Mach-Zender intensity modulator (IM) which pulses the light at an a pulse width and repetition period set by an RF pulse generator. In this experiment, the

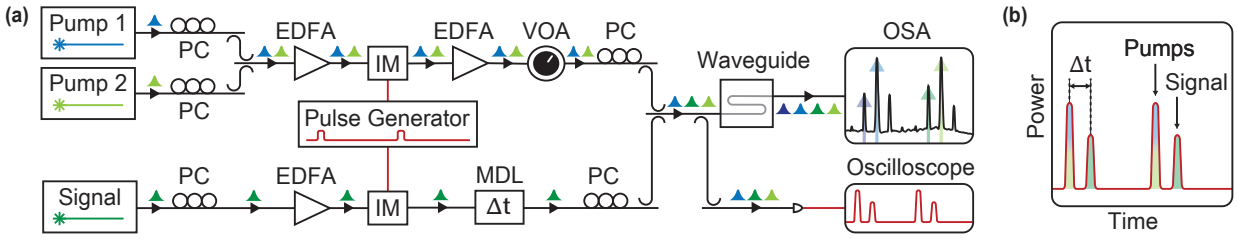

Figure 2.1 Experimental Layout. ***(a)*** *Laser light from two pump lasers passes through individual polarization controllers (PC) and is combined. The combined pump light is amplified with an erbium doped fiber amplifier (EDFA) before passing through an optical intensity modulator (IM) which generates pulses determined by an RF pulse generator. The same process occurs for a signal laser at a different frequency. After modulation, the pumps are amplified again with an EDFA, then pass through a variable optical attenuator (VOA). The signal passes through a delay line (MDL), allowing the signal pulses to be delayed. After additional PCs, the signal and pumps are combined and coupled onto an integrated silicon waveguide on the chip. Bragg Scattering Four-Wave Mixing (BSFWM) and other nonlinear mixing occurs in the silicon waveguide, generating wavelengths which are visible on an Optical Spectrum Analyzer (OSA). An oscilloscope aids pump and signal pulse synchronization.* ***(b)*** *A visualization of pump power vs time, showing the pump and signal pulses with a gap Δt (not at alignment). This gap could be adjusted from -280 ps to +280 ps using the MDL.*

pulse widths were 150 ps and the repetition period was 6.98 ns. An identical source (the signal) emits light at 1558 nm which passes through its own PC, EDFA, and IM (connected to the same RF pulse generator). The signal pulses then pass through a manual delay line (MDL) to allow an optical delay from -280 to +280 ps, followed by an additional PC. The pulses from the two pumps pass through an additional EDFA, bringing their combined average power to 26 dBm, followed by a variable optical attenuator (VOA) and PC. The pumps and signal are finally combined and coupled into the silicon chip, while 1% of the light is routed to an oscilloscope with a fiber optic input port to verify time-synchronization of pumps and signal pulses. Bragg Scattering Four-Wave Mixing (BSFWM) and other nonlinear mixing processes occur on the silicon chip. Finally, the combined light exiting the chip (with pump and signal pulses still with 150 ps pulse widths) is measured (as an average light intensity) on an optical spectrum analyzer (OSA).

2.1.1 Pulse Extinction

It is critical to measure the extinction of the pulses produced by the source. Extinction is the ratio of pulse height to background height; it measures how well the optical signal is all the way "on" during the pulse duration and completely "off" throughout the rest of the duty cycle. For example, a 20 dB extinction implies that the level of optical power during the pulse is a factor of 100 greater than what it is when the pulse is "off." A perfect pulse would be fully "on" during the pulse duration but completely "off" (zero power) the remainder of the time; its extinction would be infinite. In this experiment, the pulse extinction measures how well the pulsed laser source avoids behaving like a continuous wave (CW) source. Extinction is therefore a direct indicator of how well the nonlinear optical loss from TPA-induced FCA will be avoided during the four-wave mixing, as discussed in Section 1.2.

Extinction is determined entirely by the performance of the Intensity Modulators (IMs), which, in this experiment, were affected by a combination of the polarization of the light entering them and an applied voltage bias from separate power supplies (not pictured in Fig, 2.1 (a)). The polarization and voltage bias were in need of frequent adjustment to maintain optimal performance.

The simplest way to measure extinction would have been to read it off from the oscilloscope by comparing the pulse height and the background height on the oscilloscope to a reference zero height. However, because of limitations in coupling the light into the oscilloscope, no reference or "true" zero was available. Rather, the pulses on the oscilloscope were centered around a "relative zero" corresponding to the average optical power input. Because no true zero was available, the power level of the background (when the pulses were "off") was not visible on the oscilloscope. Instead, the extinction was estimated and monitored using power meters located after the IMs, tapping into the system through 99-1 fiber couplers (not pictured in (Fig, 2.1 (a)). Details on the extinction calculation and mathematical derivations using this approach are described in Appendix A.

2.2 A Low-Loss Silicon Waveguide for High-Efficiency BSFWM

The silicon-on-insulator waveguide that was used in this experiment was specially designed to have minimal linear loss at telecom wavelengths. The geometry of this waveguide has been shown to reduce loss.

Light was coupled onto the waveguide using a grating coupler device on the silicon chip such that incident light normal to the chip surface was captured and routed into the waveguide. Light exiting the waveguide was emitted with an identical grating coupler operating in reverse. Inefficient coupling from the optical fibers onto the chip (and vice versa) was the greatest single source of loss, contributing a minimum of approximately 10 dB of loss at each coupling. This loss could be minimized through careful adjustment of fiber stages. Prior to data collection, loss across the entire chip was measured using a CW source to estimate the coupling loss and on-chip power levels.

2.3 Data Collection and Processing

Because of the broad tunability of the pulsed source, we had the ability to take data across a wide range of parameters. This customizability enables a degree of FWM characterization not available with more limited laser sources. The tunability we had available included laser wavelengths from 1530 nm to 1565 nm for each of the pumps and the signal; pulse widths from as short as 100 ns; repetition periods as short as 100 ns to 200 ns; optical delays between the pulses of $\pm$280 ps to allow full, partial, or no temporal pulse alignment; partial or full attenuation of the pump pulses; and pulse extinction upwards of 20 dB, adjusted using the RF pulse generator output voltage and the optical polarizations of the pumps and signal. To illustrate the wide characterization available, we measure BSFWM effects across a sweep of two parameters, namely the pump power and the temporal synchronization between the signal pulse and the pump pulses.

Measurements were taken from the OSA through a semi-automated process. Before taking data, coupling loss across the silicon chip was estimated using a continuous wavelength (CW) source. Additionally, the pulse extinction was estimated for both the signal and the pumps by recording their average power at two pulse widths (see Appendix A for details on extinction calculation). Then, the at maximum pump power (minimal attenuation on the VOA), data was read automatically from the OSA at fifteen signal pulse delay (Δt) values from -280 ps to +280 ps. The pump power was then reduced slightly and data was again read automatically at the same fifteen Δt values. This process was repeated at fifteen pump attenuation levels until the pumps were completely attenuated.

A MATLAB algorithm was used to find the peaks in the OSA spectra corresponding to the powers of the pumps, idler, and signal at each mean pump power P_p and signal pulse delay Δt value. The values were adjusted to account for loss through the fiber leading from the chip to the OSA and the coupling loss at the chip output. It was assumed that half of the coupling loss of the chip occurred at the input coupler and half at the output. The values were also adjusted to represent the peak pulse powers (rather than average powers measured by the OSA) using the extinction calculations described in Appendix A.

2.4 Results

Relying on the capabilities of the tunable pulsed source, we observed record high frequency conversion efficiency for BSFWM in an CMOS-compatible integrated silicon platform.

2.4.1 Conversion Efficiency

In this work, the "conversion efficiency" from the signal to the idler frequency—at a chosen mean pump power P_P and signal pulse delay Δt—refers to the ratio (or logarithmic difference) between the measured output power of the signal at very weak pump powers (when conversion to the idler

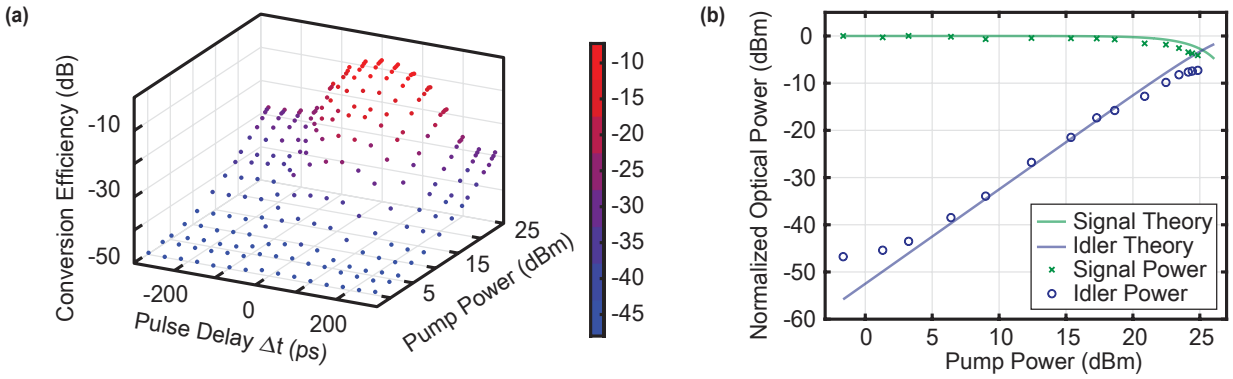

Figure 2.2 Results. ***(a)*** *Conversion efficiency (equivalent to normalized idler power) from the signal frequency to idler frequency, as a function of pump power and time-delay Δt of the signal light.* ***(b)*** *Optical power at signal and idler frequencies as functions of total pump power. The theoretical signal and idler powers are shown, demonstrating good agreement above the noise threshold at a nonlinear Kerr coefficient of $\gamma = 60\ W^{-1}m^{-1}$. The deviation at high pump powers is explained in the text.*

is next to none) and the measured output power of the idler at the chosen pump power. Because because the ratio is not taken using the signal *input* power, this definition of conversion efficiency is not the same as the *system* efficiency (comparing total input signal power to the output idler power), which was not measured in this work. Rather, this is an *effective* or *useful* conversion efficiency. This definition automatically corrects for linear loss in the waveguide. However, it does not correct for nonlinear loss, as will be discussed below.

A plot of idler powers is shown in Fig. 2.2 (a) at discrete values of Δt and P_P. In this plot, the signal input power (in dBm) was subtracted from each idler power value so that the vertical axis corresponds to the conversion efficiency described in the previous paragraph. These results correspond to a pulse width of 150 ps with a pulse repetition period of 6.98 ns. As noted on the plot, the peak conversion efficiency measured was -7.29 dB or 18.7%.

To the best of our knowledge, this is the highest experimentally demonstrated BSFWM conversion efficiency in a CMOS-compatible integrated silicon waveguide. For example, 12% conversion efficiency was reported in 2016 in a silicon on insulator platform [10] and 5% using an asymmetrical pumping scheme [11]. 15% conversion efficiency was reported in a hydrogenated amorphous

silicon (a-Si:H) platform in 2017 [12]. Bell 2016 [10] and Li 2017 [12] also report even higher conversion efficiencies than those just listed by mathematically compensating for the linear or nonlinear propagation loss in the waveguide. However, we instead focus on the effective or useful conversion efficiency which is the idler power actually received at the waveguide output as a fraction of the signal power which is received in the absence of pumps, without mathematical adjustments that would increase the reported efficiency. However, comparison to their original results listed above demonstrates the record-level efficiency we observed through the pulsed-source method used in this experiment.

2.4.2 Fit to Theory

The equations of motion describing the BSFWM process in this experiment are derived in the supplementary material of Otterstrom 2021 [2]. The equations lead to an expression for the signal to idler conversion efficiency as a function of distance z traversed in the waveguide (Equation 4 in Otterstrom [2]):

$$\varepsilon = |\kappa|^2 \frac{\sin^2(z\sqrt{\delta\beta^2 + |\kappa|^2})}{\delta\beta^2 + |\kappa|^2}. \tag{2.1}$$

Here, $\kappa = 2\gamma\sqrt{P_p^{(1)} P_p^{(2)}}$, where γ is the Kerr coefficient which quantifies the strength of the BSFWM coupling, and $P_p^{(1)}$ and $P_p^{(2)}$ are the pump powers. In this experiment, the phase mismatch $\delta\beta$ between the relevant wavelengths (signal, idler, and pumps) is minimal and can be approximated as $\delta\beta \approx 0$. Additionally, the pump powers are approximately equal and we can estimate $\sqrt{P_p^{(1)} P_p^{(2)}} \approx P_p$ (where P_p is the mean pump power). With these approximations, the conversion efficiency expression in Equation 2.1 becomes

$$\varepsilon = \sin^2(2\gamma P_p z). \tag{2.2}$$

Similarly, the simplified equation for the signal power as a function of P_p is

$$P_S = \cos^2(2\gamma P_p z). \tag{2.3}$$

These are plotted as the solid lines in Fig. 2.2, alongside the experimental results at signal delay $\Delta t = 0$. The conversion efficiency is labeled "Idler Power" because the idler power normalized to the weak-pump signal power is exactly the conversion efficiency we are interested in, as described in Section 1.2. The Kerr coefficient of best fit, shown in this plot, was $\gamma = 60$ W^{-1} m^{-1} which is consistent with the waveguide geometry and optical modes.

Fig. 2.2 (b) shows good experimental agreement with theory in the central portion (medium pump powers). The deviation of the experimentally measured idler power at weak pump levels is an artifact of the experimental noise floor. At high pump powers, the theoretical fits are noticeably higher than the experimental data. In the case of the idler, the deviation from the theoretical fit is primarily due to nonlinear loss in the waveguide, which becomes prevalent at higher powers. The nonlinear loss occurs from two-photon absorption (TPA) and TPA-induced free carrier absorption (FCA) (as discussed in Section 1.2.2); not all of that loss could be avoided through the pulsed-source technique used in this experiment. The idler power does not become high enough for it to experience its noticeable parasitical FWM processes. In the case of the signal, the additional loss is due a combination of nonlinear loss and parasitical FWM processes. The parasitical FWM processes affecting the output signal power include the modulation interaction (two signal photons producing sidebands above and below the signal frequency) and phase-conjugation processes (two pump photons producing a signal and idler photon). These processes are described in greater detail in McKinstrie 2005 [5]. The modulation interaction removes signal photons while phase conjugation adds signal photons, thus resulting in a net deviation for the signal that is smaller than the deviation seen for the idler, as visible in Fig. 2.2 (b).

Chapter 3

Conclusion and Discussion

In this thesis, we demonstrate that the efficiency of optical frequency conversion via BSFWM in silicon can be dramatically improved. This is achieved through an ultrafast pulsing technique that reduces nonlinear loss from TPA-induced FCA. To allow detailed characterization of the BSFWM processes, we build a highly-customizable pulsed source. We demonstrate that this source is capable of producing pulses with durations as short as 150 ps, extinctions upwards of 25 dB, and peak pulse powers near 1 W. Additionally, the source allows manipulation of a multitude of parameters not available in commercial sources, enabling a broad characterization of nonlinear optical processes.

We demonstrate that the pulsed source is capable of producing sufficiently short, high-power pulses to realize high-efficiency BSFWM frequency conversion. We demonstrate record-level conversion efficiency for BSFWM in a CMOS-compatible silicon platform as high as 18% (without mathematically adjusting for linear or nonlinear loss). We also show the pulsed source allows broad characterization of BSFWM across multiple parameters. Specifically, we vary the mean pump power P_p and the signal delay Δt.

These results show experimentally that unity-level frequency conversion via BSFWM in a CMOS-compatible platform is within reach using this technique. Reduction in the sources of loss, especially the coupling onto and off of the silicon chip, would provide the largest step towards

achieving this result. Near-unity frequency conversion is an important step towards useful integrated photonics applications.

Appendix A

Pulse Extinction Calculations

As discussed in 2.1.1, in this experiment it is crucial to know the pulse extinction (the ratio between pulse height and background height) of both the signal and the pumps. This need arises because the optical spectrum analyzer (OSA) and other power measurement instruments are only capable of measuring the *average* power. When a measurement is taken, some fraction of the measured average power is delivered during the short time that the pulse is "on" (within the pulse itself) and the remaining power is delivered during the time the pulse is "off" (within the pulse background). Perfect instruments would of course generate pulses that switched completely "on" and "off" and *all* of the average power would be delivered during the pulse itself. In practice, however, with duty cycles around 2% it was not uncommon for us to observe (especially when the instruments were in want of tuning or calibration) that 50% or more of the average power was being delivered during the pulse background rather than during the pulse duration itself.

If the pulse extinction is known, two critical pieces of information can be accurately estimated. The first is the fractional powers just discussed. The second is the *peak* pulse power (the pulse "height" on a power vs. time plot). With these two pieces of information, the conversion efficiency can finally be accurately calculated.

In this appendix, I first show how the extinction of the signal pulses was calculated from directly the data we gathered (Section A.1). This calculation was possible because of the wide tunability of the pulsed source (see Section 1.3). Next, I discuss a geometric model of pulse extinction and derive an expression for estimating the pulse extinction based on measurements of the average power at two known pulse widths (Section A.2). In Section A.3, I discuss a significant inaccuracy of the model which arose from a deficiency in our pulse generator. I then discuss the calibration of the model with the signal pulse extinction and our use of the calibrated model to accurately estimate the extinction of the pump pulses.

A.1 Calculating the Signal Extinction From the OSA Data

One of the benefits of the wide tunability (see Section 1.3) of the pulsed source we developed was the ability to estimate the extinction of the signal from the OSA data itself. This was possible because data could be gathered across a range of signal pulse delay values (Δt) using the tunable delay line (see Section 2.1). We did not have this ability with the pumps, which will be discussed in the following sections.

Finding the signal pulse extinction begins with an understanding of the four-wave mixing which occurs on the chip when the pump and signal pulses are completely *aligned* ($\Delta t = 0$) vs *misaligned* in time ($|\Delta t|$ maximum, or about 280 ps in our experiment). When the pump and signal pulses are aligned, nearly all of the idler power is generated through the mixing of the peak pump power with the peak signal power, or in other words during the time when the pulses are both "on." Almost no idler power is generated during the period when both pump and signal pulses are "off" (pump background mixing with idler background).

When the pulses are misaligned, the situation is more complicated. Even though the peak pump power cannot mix with the peak signal power, some BSFWM still occurs, resulting in some

measurable idler generation. The origin of the idler generation is threefold. First, there is the background (pulse "off") pump power mixing with the background signal power. Although this contribution is largest in the time domain, it contributes an extremely small fraction of the average generated idler power. Second, there is the background pump power mixing with the peak (pulse "on") signal power. This contribution is potentially noticeable, but still small because of the weak pump background power level (see 2.4.2). Third, there is the four-wave mixing between the peak (pulse "on") pump power and the background signal power. This is the largest contribution by far, because of the high peak pump power during this time. To a good approximation, we can ignore the idler generation from the other two effects and approximate that all of the idler generation results from the mixing of the peak pump power and the background signal power.

As just outlined, when $|\Delta t|$ is large (pulses misaligned), the only significant contribution to idler power generation is the *background* signal power mixing with the peak pump power. In contrast, with $\Delta t = 0$, the only significant contribution is *peak* signal power mixing with the peak pump power. This provides a technique for calculating the signal extinction. If all parameters besides Δt are held constant, including the average signal power, the ratio between the measured idler power at $\Delta t = 0$ versus at $|\Delta t| \approx 280\ ps$ will be approximately equal to the ratio between the background signal power P_{bg} and the peak signal power P_{pk}. This ratio is precisely the signal pulse extinction we seek: $\varepsilon = P_{pk}/P_{bg}$. In this experiment, the signal extinction was found to be:

$$\varepsilon_S = 133.3 = 21.25\ dB \tag{A.1}$$

A.2 A Geometric Model of Pulse Extinction

With the signal extinction calculated, we turn to the calculation of pump extinction. However, because idler generation with pulses misaligned ($|\Delta t|$ maximum) is primarily due to the mixing

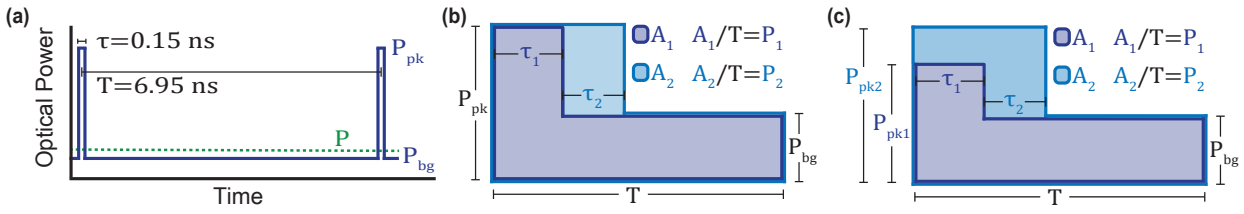

Figure A.1 Pulse Extinction Models. ***(a)*** *Cartoon drawing of an idealized rectangular pulse, drawn to scale in the time dimension for the pulse widths used in this experiment. Key variables are shown, including the power level of the peak P_{pk}, the power level of the background P_{bg}, the average power P (experimentally measurable by power meters), and the pulse width τ. The extinction is given by $\varepsilon = P_{pk}/P_{bg}$.* ***(b)*** *Idealized rectangular pulse with proportions inflated to emphasize key parameters. Pulse is shown at two different pulse widths τ_1 and τ_2. Additionally, the background power P_{bg}, pulse peak power P_{pk}, and pulse period T are shown. Two geometric areas are of interest, the area made up of the first pulse and its background A_1, and the area of the second pulse and its background, A_2. The average powers for the two pulses (the known, experimentally measurable powers) are not shown, but are given by $P_1 = A_1/T$ and $P_2 = A_2/T$.* ***(c)*** *Idealized rectangular pulse at two pulse widths, with a change in peak power also introduced, as discussed in Sec A.3. The parameters P_{pk1} and P_{pk2} replace the simpler P_{pk}, but otherwise the parameters remain the same.*

of peak pulse power (see the previous section A.1), the generated idler power cannot be used as an indicator of the *pump* extinction in the same way in which it was used for the *signal* extinction. Instead, we develop a general geometric model of pulse extinction.

This model depends critically on two measured values that do not appear explicitly in the data gathered from the optical spectrum analyzer (OSA): the average power at two distinct, known pulse widths (or duty cycles). We call these pulse durations τ_1 and τ_2 and the measured average powers P_1 and P_2. Measurements of these average powers (for both the pumps and the signal) were taken just before collecting OSA data in this experiment.

The geometric model of the pulse extinction is shown in Fig. A.1 (b) at the two pulse widths. The pulse repetition period, T, is the same for both pulse widths ($T = 6.98\ ns$ in our experiment). The duty cycles of the pulses at the two pulse widths are known ($c_1 = \tau_1/T$ and $c_2 = \tau_2/T$). The measured average powers P_1 and P_2 are represented by the total shaded area divided by the period ($P_1 = A_1/T$ and $P_2 = A_2/T$) . The peak pulse power is P_{pk} and the background power is P_{bg}. We make the assumption that the peak power and background power remain constant when switching from pulse width τ_1 to pulse width τ_2. This assumption turned out to be partially incorrect, as will

be discussed in section A.3. The ratio between peak power and background power $\varepsilon = P_{pk}/P_{bg}$ is the pulse extinction we want to find (in terms of the known values P_1, P_2, c_1, and c_2).

A.2.1 Expression for the Extinction

It is easy to see that the areas can be written as $A_1 = P_{pk}\tau_1 + P_{bg}T - P_{bg}\tau_1$ and $A_2 = P_{pk}\tau_2 + P_{bg}T - P_{bg}\tau_2$. We take their ratio and re-express it in terms of the experimentally known values P_1, P_2, c_1, and c_2 to solve for the extinction ratio $\varepsilon = P_{pk}/P_{bg}$:

$$\frac{A_1}{A_2} = \frac{P_{pk}\tau_1 + P_{bg}T - P_{bg}\tau_1}{P_{pk}\tau_2 + P_{bg}T - P_{bg}\tau_2}$$

Cross-multiplying, then dividing the equation by T^2 and P_{bg} (and substituting ε for the ratio P_{pk}/P_{bg}:

$$\begin{aligned} A_1\left(P_{pk}\tau_2 + P_{bg}T - P_{bg}\tau_2\right) &= A_2\left(P_{pk}\tau_1 + P_{bg}T - P_{bg}\tau_1\right) \\ \frac{A_1}{T}\left(\frac{P_{pk}}{P_{bg}}\frac{\tau_2}{T} + 1 - \frac{\tau_2}{T}\right) &= \frac{A_2}{T}\left(\frac{P_{pk}}{P_{bg}}\frac{\tau_1}{T} + 1 - \frac{\tau_1}{T}\right) \\ P_1(c_2\varepsilon + 1 - c_2) &= P_2(c_1\varepsilon + 1 - c_1) \end{aligned}$$

Solving for the extinction ε:

$$\begin{aligned} \varepsilon(P_1c_2 - P_2c_1) &= P_1(c_2 - 1) - P_2(c_1 - 1) \\ \varepsilon &= \frac{P_1(c_2 - 1) - P_2(c_1 - 1)}{P_1c_2 - P_2c_1} \end{aligned} \tag{A.2}$$

A.3 Calculating the Pump Extinction Using the Model

If the geometric model just discussed is accurate, then Eq A.2 is an expression for the extinction of any pulse (pumps or signal) in terms of the known values c_1, c_2, P_1, and P_2. However, a verification with real data from the pulsed source and power meters showed that the model was not accurate for

short initial pulse durations (short τ_1). Additional testing revealed that at very short pulse durations ($\leq$ 150 ps, such as those used to gather the BSFWM data in this experiment) the pulse generator did not produce pulses that reached the full pulse height (peak power). So, when transitioning from the first duty cycle c_1 to the second c_2, if the initial pulse width τ_1 was short then the pulses not only increased in width but also in height.

To accommodate this pulse height variation, we revise the geometric model to include both a change in pulse width *and* a change in the pulse height. This is represented in Fig. A.1 (c), where the two peak heights are drawn as P_{pk1} and P_{pk2}. Since the experimental data was taken at the first pulse width (150 ps), in this new model the desired extinction of the pumps is given by $\varepsilon_P = P_{pk1}/P_{bg}$.

The change in pulse height introduces an additional unknown and leaves the system unsolvable in the case of the pumps. However, in the case of the signal, the extinction and the first pulse width $\varepsilon_S = P_{pk1}/P_{bg}$ is not an unknown, but can be found using the experimental data as described in Sec A.1 and given by Eq A.1. This allows us to solve for the unknown P_{pk2} for at least the signal pulses.

However, rather than solve directly for P_{pk2} for the signal, we make the assumption that the *fractional* change in pulse height P_{pk2}/P_{pk1} is the same for both the signal pulses and the pump pulses. We then use this value to find the desired extinction $\varepsilon_P = P_{pk1}/P_{bg}$ of the pumps.

To find the fractional change in pulse height P_{pk2}/P_{pk1}, we use a similar approach as in the previous section, beginning with expressions for the areas: $A_1 = P_{pk1}\tau_1 + P_{bg}T - P_{bg}\tau_1$ and $A_2 = P_{pk2}\tau_2 + P_{bg}T - P_{bg}\tau_2$. If we solve both expressions for $P_{pk1}\tau_1$ and $P_{pk2}\tau_2$, we have:

$$P_{pk1}\tau_1 = A_1 - P_{bg}T + P_{bg}\tau_1$$

$$P_{pk2}\tau_2 = A_2 - P_{bg}T + P_{bg}\tau_2$$

Dividing by T and writing in terms of the known values c_1, c_2, P_1, and P_2:

$$P_{pk1}c_1 = P_1 - P_{bg} + P_{bg}c_1$$

$$P_{pk2}c_2 = P_2 - P_{bg} + P_{bg}c_2$$

We are still left with the unknowns P_{pk1}, P_{pk2}, and P_{bg}, which we need to write in terms of the signal extinction $\varepsilon_S = P_{pk1}/P_{bg}$ and the ratio we want to solve for P_{pk2}/P_{pk1}. Dividing both equations by P_{pk1} and writing in terms of ε_S, the two equations become:

$$c_1 = \frac{P_1}{P_{pk1}} - \frac{1}{\varepsilon_S} + \frac{1}{\varepsilon_S}c_1$$
$$\frac{P_{pk2}}{P_{pk1}}c_2 = \frac{P_2}{P_{pk1}} - \frac{1}{\varepsilon_S} + \frac{1}{\varepsilon_S}c_2$$

Then we solve the first equation for P_{pk1} in terms of known values, and the second equation for the ratio we seek P_{pk2}/P_{pk1}:

$$P_{pk1} = \frac{P_1\varepsilon_S}{1 - c_1 + c_1\varepsilon_S}$$
$$\frac{P_{pk2}}{P_{pk1}} = \frac{1}{c_2}\left(\frac{P_2}{P_{pk1}} - \frac{1}{\varepsilon_S} + \frac{1}{\varepsilon_S}c_2\right)$$

Finally we substitute the first equation into the second and simplify to find:

$$\frac{P_{pk2}}{P_{pk1}} = \frac{P_1(c_2 - 1) + P_2 + P_2c_1(\varepsilon_S - 1)}{P_1c_2\varepsilon_S} \tag{A.3}$$

In this experiment, the fractional change in pulse height for the signal pulses was:

$$\frac{P_{pk2}}{P_{pk1}} = 1.226 \tag{A.4}$$

or a 22.6% increase in pulse height from the first pulse width τ_1 to the second τ_2.

Now that the fractional change in pulse height between the two pulse widths is known, we can solve for the extinction of the pumps $\varepsilon_P = P_{pk1}/P_{bg}$. The problem has already been essentially solved. We begin with Eq A.3, replace ε_S with ε_P, and solve for ε_P in terms of P_{pk2}/P_{pk1}:

$$\varepsilon_P = \frac{P_1(c_2 - 1) - P_2(c_1 - 1)}{(P_{pk2}/P_{pk1})P_1c_2 - P_2c_1} \tag{A.5}$$

Comparison with Eq A.2 reveals a very similar expression. Using Eq A.5, the measured value for the pump extinction using the 150 ps pump pulses in this experiment was:

$$\varepsilon_P = 44.20 = 16.45 \text{ dB} \tag{A.6}$$

Bibliography

[1] N. T. Otterstrom *et al.*, "Backscatter-Immune Injection-Locked Brillouin Laser in Silicon," Phys. Rev. Appl. **14,** 044042 (2020).

[2] N. T. Otterstrom *et al.*, "Nonreciprocal Frequency Domain Beam Splitter," Phys. Rev. Lett. **127,** 253603 (2021).

[3] K. Li, Ph.D. thesis, The John Hopkins University, 2018.

[4] G. Agrawal, *Nonlinear Fiber Optics* (Elsevier, 2013).

[5] C. J. McKinstrie, J. D. Harvey, S. Radic, and M. G. Raymer, "Translation of quantum states by four-wave mixing in fibers," Optics Express **13,** 9131 (2005).

[6] R. W. Boyd, *Nonlinear Optics* (Elsevier, 2008).

[7] E. A. Kittlaus, H. Shin, and P. T. Rakich, "Large Brillouin amplification in silicon," Nature Photonics **10,** 463–467 (2016).

[8] Q. Xu, V. R. Almeida, and M. Lipson, "Time-resolved study of Raman gain in highly confined silicon-on-insulator waveguides," Optics Express **12,** 4437 (2004).

[9] T. K. Liang and H. K. Tsang, "Efficient Raman amplification in silicon-on-insulator waveguides," Applied Physics Letters **85,** 3343–3345 (2004).

[10] B. A. Bell, J. He, C. Xiong, and B. J. Eggleton, "Frequency conversion in silicon in the single photon regime," Optics Express **24,** 5235 (2016).

[11] Y. Zhao, D. Lombardo, J. Mathews, and I. Agha, "Low control-power wavelength conversion on a silicon chip," Optics Letters **41,** 3651 (2016).

[12] K. Li, H. Sun, and A. C. Foster, "Four-wave mixing Bragg scattering in hydrogenated amorphous silicon waveguides," Optics Letters **42,** 1488 (2017).

Index